Nonequilibrium lateral force and torque by thermally excited nonreciprocal surface electromagnetic waves

Chinmay Khandekar,[1,*] Siddharth Buddhiraju◉,[1] Paul R. Wilkinson,[2] James K. Gimzewski,[2] Alejandro W. Rodriguez,[3] Charles Chase◉,[4] and Shanhui Fan[1,†]

[1]*Department of Electrical Engineering, Stanford University, California 94305, USA*
[2]*Department of Chemistry and Biochemistry, University of California Los Angeles, Los Angeles, California 90095, USA*
[3]*Department of Electrical and Computer Engineering, Princeton University, Princeton, New Jersey 08544, United States*
[4]*UnLAB, Savannah, Georgia 31405, USA*

We show that an isotropic dipolar particle in the vicinity of a substrate made of nonreciprocal plasmonic materials can experience a lateral thermal-fluctuations-induced force and torque when the particle's temperature differs from that of the slab and the environment. We connect the existence of the lateral force to the asymmetric dispersion of nonreciprocal surface polaritons and the existence of the lateral torque to the spin-momentum locking of such surface waves. Using the formalism of fluctuational electrodynamics, we show that the features of lateral force and torque should be experimentally observable using a substrate of doped indium antimonide (InSb) placed in an external magnetic field, and for a variety of dielectric particles. Interestingly, we also find that the directions of the lateral force and the torque depend on the constituent materials of the particles, which suggests a sorting mechanism based on nonequilibrium fluctuational electrodynamics.

I. INTRODUCTION

Nonreciprocal electromagnetic surface waves can occur at an interface between two semi-infinite bulk regions, at least one of which breaks reciprocity. Notable examples include surface waves at the interface between gyrotropic medium and regular dielectric as well as one-way edge modes at the interface between electromagnetic analogues of topological and regular insulators [1–6]. In many cases, the existence of such nonreciprocal surface states is linked with the nontrivial topological behavior of the bulk region making them fundamentally intriguing [7–9]. They are also useful for practical devices like isolators, circulators, phase shifters, and lasers [10,11].

In this paper, we show that the nonreciprocal surface waves have intriguing fundamental implications for nonequilibrium fluctuational electrodynamics [12,13]. As illustrated in Fig. 1, we consider an exemplary system comprising a reciprocal nanoparticle in the vicinity of a gyrotropic plasmonic substrate, consisting of a doped InSb slab in the presence of a magnetic field applied parallel to its surface (along x-axis). The slab supports nonreciprocal surface plasmon polaritons (SPPs) whose asymmetric dispersion ($\omega(\mathbf{k}) \neq \omega(-\mathbf{k})$) is depicted in the inset under a Voigt configuration. These SPPs carry not only linear momentum but also spin angular momentum locked transverse to the linear momentum [14,15]. When the particle's temperature (T_p) differs from the temperature of its surroundings including the slab (T_e), there is a net

exchange of thermal-fluctuations-generated photons between the particle and the nonreciprocal SPPs. Since the resulting exchange of linear momentum and spin angular momentum is asymmetric with respect to forward and backward SPPs, we find that the particle experiences a lateral nonequilibrium force (F_y) transverse to applied magnetic field, and a lateral nonequilibrium torque (M_x) parallel to magnetic field.

We provide a rigorous fluctuational electrodynamic analysis of these effects applicable to a particle in the vicinity of a bianisotropic substrate, not limited to the Voigt configuration of the schematic. Instead of the usual trace formulas in Casimir physics, we provide semi-analytic expressions for force and torque, which are more transparent in capturing the flow of energy, linear and angular momenta between the particle and the SPPs. Using these expressions, we prove that a lateral force and torque on an isotropic particle are not possible for reciprocal substrate, or for either reciprocal or nonreciprocal substrate under equilibrium condition ($T_p = T_e$).

Moreover, since the particle interacts with large wavevector SPPs where nonlocal dielectric response cannot be ignored, we use a nonlocal hydrodynamic magnetoplasma model of InSb, which indicates the absence of strictly unidirectional SPPs [16]. Our calculations show that the lateral force and torque arise because of nonreciprocity, and do not require strictly unidirectional states. We also clarify that our analysis incorporates both thermal fluctuations and quantum (zero-point) fluctuations of photons. However, the contribution of quantum fluctuations to the effects discussed in this paper is either zero or negligible compared to the contribution of thermal fluctuations. Therefore, although our theory captures Casimir physics for general situations involving thermal

---
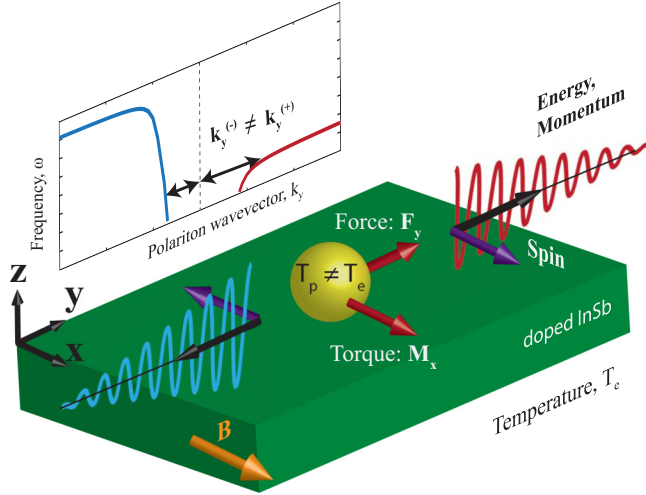*ckhandek@stanford.edu
†shanhui@stanford.edu

FIG. 1. We illustrate nonequilibrium lateral force and torque on an isotropic dipolar nanoparticle in the near field of a doped InSb slab placed in magnetic field parallel to its surface. We assume a static magnetic field is applied along **x** axis of the geometry and clarify the asymmetric interaction of the particle with nonreciprocal SPPs of the slab along **y** axis (Voigt configuration). The asymmetric dispersion shown in the inset reveals the unequal magnitude of linear momentum for forward and backward SPPs of equal frequency. The SPPs also carry transverse spin angular momentum locked to their momentum as displayed. When the particle's temperature T_p is different from the temperature T_e of the rest of the system, the net exchange of linear and spin angular momentum via fluctuations-generated photons is asymmetric with respect to forward and backward SPPs causing a lateral force transverse to applied field (F_y) and a lateral torque parallel to applied field (M_x).

nonequilibrium, we avoid identifying the discussed fluctuational phenomena as Casimir effects since they primarily rely on the differences in thermal fluctuations at nonzero temperatures.

Fluctuational electrodynamics of nonreciprocal systems is an emerging research topic with recent theoretical proposals for new fundamental effects [17–20] and practical applications [21–24] related to thermal radiation and radiative heat transfer. Other related works explored the effects of nonreciprocity on fluctuations-induced torque and force for quantum optical systems like excited atoms [25,26], force between closely separated plates [27,28], and torque for a single isolated sphere [29] or closely-separated nanoparticles [30]. However, the important fundamental connection between the asymmetric properties of nonreciprocal surface waves and the behaviors of these nonequilibrium fluctuational forces and torques has not been discussed previously. Our

paper thoroughly explains this connection. Moreover, controlled experiments probing these effects of nonreciprocity are quite challenging. For example, for the well-known plate-plate geometry [27,28], these effects are quite weak due to the large inertia of the bulk plates. In contrast, our concrete predictions for a sphere-plate geometry indicate that these effects can be readily detected in modern Casimir [12,13,25] and nanoscale heat transfer [31,32] experiments. We also reveal interesting dependence of directionalities of the lateral features on the material composition of the particle. We note that the lateral Casimir forces for equilibrium systems have been studied previously in Refs. [33–37]. In these systems, lateral force can only arise from nonuniform lateral configurations. In contrast, lateral nonequilibrium fluctuational force in our nonreciprocal system can arise despite the translational invariance of the substrate in the lateral directions.

II. THEORY

We consider a dipolar particle characterized by isotropic polarizability tensor $\alpha_{jk} = \alpha_0 I_{3\times3}$ and placed at a distance d from a generic bianisotropic planar substrate. The particle is at temperature T_p and the entire environment surrounding the particle, including the substrate and the vacuum half-space, is at temperature T_e. Using fluctuational electrodynamics, the spectral densities of the net power transfer from the particle to the environment $P(\omega)$, the force $F_j(\omega)$ and the torque $M_j(\omega)$ on the particle for $j = [x, y, z]$ are [36,38]

$$P(\omega) = \omega \text{Im}\left[\langle p_j^{\text{fl}*}(\omega)E_j^{\text{ind}}(\omega)\rangle + \langle p_j^{\text{ind}*}(\omega)E_j^{\text{fl}}(\omega)\rangle\right], \quad (1)$$

$$F_j(\omega) = \text{Re}\left[\langle p_k^{\text{fl}}(\omega)\partial_j E_k^{\text{ind}*}(\omega)\rangle + \langle p_k^{\text{ind}}(\omega)\partial_j E_k^{\text{fl}*}(\omega)\rangle\right], \quad (2)$$

$$M_j(\omega) = \varepsilon_{jkl}\text{Re}\left[\langle p_k^{\text{fl}}(\omega)E_l^{\text{ind}*}(\omega)\rangle + \langle p_k^{\text{ind}}(\omega)E_l^{\text{fl}*}(\omega)\rangle\right], \quad (3)$$

where Einstein summation convention is used with $j, k, l \in [x, y, z]$. $\langle\cdots\rangle$ denotes statistical ensemble average of the fluctuating quantities enclosed within. These physical quantities are expressed in SI units and the total power, force, and torque are obtained by integrating over both positive and negative frequencies as $Q^t = \int_{-\infty}^{\infty} Q(\omega)d\omega/2\pi$ where $Q = \{P, F_j, M_j\}$. Here $p_j^{\text{ind}} = \epsilon_0 \alpha_{jk} E_k^{\text{fl}}$ is the dipole moment induced in the particle by the environment field fluctuations. E_j^{ind} is the field at the dipole location by the fluctuating dipole moment itself. In general, the field $E_j^{\text{ind}}(\mathbf{r}_2, \omega)$ at an arbitrary location $\mathbf{r}_2$ generated by the dipole moment $p_j^{\text{fl}}(\mathbf{r}_1, \omega)$ at the spatial position $\mathbf{r}_1$ is given by $E_j^{\text{ind}}(\mathbf{r}_2, \omega) = \omega^2 \mu_0 G_{jk}(\mathbf{r}_2, \mathbf{r}_1, \omega)p_j^{\text{fl}}(\mathbf{r}_1, \omega)$ where $G_{jk}(\mathbf{r}_2, \mathbf{r}_1, \omega)$ is the Green's function. The semi-analytic form of Green's function in the dipole-plate geometry considered here has been previously derived [19]. Its simplified form as a summation over plane waves is $\overline{\overline{G}}(\mathbf{r}_1, \mathbf{r}_2, \omega) = \int \frac{d^2\mathbf{k}_\parallel}{(2\pi)^2}\overline{\overline{G}}_\mathbf{k}(\mathbf{r}_1, \mathbf{r}_2, \omega)$ where

$$\overline{\overline{G}}_\mathbf{k} = e^{i\mathbf{k}_\parallel \cdot (\mathbf{R}_1 - \mathbf{R}_2)}\frac{i}{2k_z}\left[\overbrace{e^{ik_z(z_1-z_2)}\left[\hat{\mathbf{e}}_{s+}\hat{\mathbf{e}}_{s+}^T + \hat{\mathbf{e}}_{p+}\hat{\mathbf{e}}_{p+}^T\right]}^{\text{vacuum part}} + \overbrace{e^{ik_z(z_1+z_2)}\left[(r_{ss}\hat{\mathbf{e}}_{s+} + r_{ps}\hat{\mathbf{e}}_{p+})\hat{\mathbf{e}}_{s-}^T + (r_{sp}\hat{\mathbf{e}}_{s+} + r_{pp}\hat{\mathbf{e}}_{p+})\hat{\mathbf{e}}_{p-}^T\right]}^{\text{reflected part}}\right]. \quad (4)$$

Here $\mathbf{r} = (\mathbf{R}, z)$ is the position vector. $\mathbf{k}_\parallel = (k_\parallel \cos\phi, k_\parallel \sin\phi)$ is the in-plane momentum such that ϕ is the angle with **x** axis of the geometry. k_z is the perpendicular wave-vector component such that $k_z^2 + k_\parallel^2 = k_0^2$ where $k_0 = \omega/c$. r_{jk} for $j, k \in [s, p]$

denotes the Fresnel reflection coefficient, which is the amplitude of j-polarized reflected light when unit-amplitude k-polarized light characterized by $(\omega, k_\parallel, \phi)$ is incident. The polarization vectors $\hat{\mathbf{e}}_{j\pm}$ for $j = [s, p]$ for waves going along $\pm\hat{\mathbf{e}}_z$ direction are:

$$\hat{\mathbf{e}}_{s\pm} = \begin{bmatrix} \sin\phi \\ -\cos\phi \\ 0 \end{bmatrix}, \quad \hat{\mathbf{e}}_{p\pm} = \frac{-1}{k_0}\begin{bmatrix} \pm k_z\cos\phi \\ \pm k_z\sin\phi \\ -k_\parallel \end{bmatrix}. \tag{5}$$

The calculation of the power, force, and torque in Eqs. (1)–(3) relies on p_j^{fl} and E_j^{fl}, which denote statistically uncorrelated particle dipole moment fluctuations and environment field fluctuations at the dipole location respectively. They satisfy the following fluctuation dissipation theorems (FDTs) based on linear response theory [39]:

$$\left\langle p_j^{\text{fl}}(\omega)p_k^{\text{fl}*}(\omega')\right\rangle = \frac{\alpha_{jk}(\omega) - \alpha_{kj}^*(\omega)}{2i}\frac{\epsilon_0}{\omega}\Theta(\omega, T_p)(2\pi)\delta(\omega - \omega'), \tag{6}$$

$$\left\langle E_j^{\text{fl}}(\mathbf{r}_1, \omega)E_k^{\text{fl}*}(\mathbf{r}_2, \omega')\right\rangle = \frac{G_{jk}(\mathbf{r}_1, \mathbf{r}_2, \omega) - G_{kj}^*(\mathbf{r}_2, \mathbf{r}_1, \omega)}{2i}\mu_0\omega\Theta(\omega, T_e)(2\pi)\delta(\omega - \omega'), \tag{7}$$

where $\langle\cdots\rangle$ denotes the statistical ensemble average and $\Theta(\omega, T) = \hbar\omega/2 + \hbar\omega/[\exp(\hbar\omega/k_B T) - 1]$ is the Planck's function giving the mean energy of a harmonic oscillator of frequency ω at thermodynamic temperature T. In the derivation of the spectral densities [Eqs. (1)–(3)] from the real-valued dipole moment $p_j(t) = \int_{-\infty}^{\infty}\frac{d\omega}{2\pi}p_j(\omega)e^{-i\omega t}$ and electric field $E_j(t) = \int_{-\infty}^{\infty}\frac{d\omega}{2\pi}E_j e^{-i\omega t}$, the factor of (2π) in the above FDTs gets canceled upon integration over frequency ω' and only equal frequency correlations survive. Using the FDTs and the Green's function, we derive the following semi-analytic expressions for the spectral densities (with intermediate steps provided in the Appendix A, B, and C):

$$P(\omega) = (\Theta_{T_p} - \Theta_{T_e})k_0^2\text{Im}\{\alpha_0(\omega)\}\left[\frac{k_0}{\pi} + \int_0^{\infty}dk_\parallel\int_0^{2\pi}d\phi\,\text{Im}\left(\frac{ik_\parallel e^{2ik_z d}}{8\pi^2 k_z}\left[r_{ss} + r_{pp}(2k_\parallel^2/k_0^2 - 1)\right]\right)\right], \tag{8}$$

$$F_x(\omega) = -(\Theta_{T_p} - \Theta_{T_e})\frac{k_0}{c}\text{Im}\{\alpha_0(\omega)\}\int_0^{\infty}dk_\parallel\int_0^{2\pi}d\phi\,\text{Im}\left(\frac{ik_\parallel e^{2ik_z d}}{8\pi^2 k_z}\left[r_{ss} + r_{pp}(2k_\parallel^2/k_0^2 - 1)\right]k_\parallel\cos\phi\right), \tag{9}$$

$$F_z(\omega) = -(\Theta_{T_p} + \Theta_{T_e})\frac{k_0}{c}\text{Im}\{\alpha_0(\omega)\}\int_0^{\infty}dk_\parallel\int_0^{2\pi}d\phi\,\text{Im}\left(\frac{ik_\parallel e^{2ik_z d}}{8\pi^2}\left[r_{ss} + r_{pp}(2k_\parallel^2/k_0^2 - 1)\right]\right), \tag{10}$$

$$M_x(\omega) = -(\Theta_{T_p} - \Theta_{T_e})\frac{k_0}{c}\text{Im}\{\alpha_0(\omega)\}\int_0^{\infty}dk_\parallel\int_0^{2\pi}d\phi\frac{k_\parallel^2}{8\pi^2 k_0}\left[\cos\phi\,\text{Im}\left\{\frac{(r_{sp} - r_{ps})e^{2ik_z d}}{k_z}\right\} + 2\sin\phi\,\text{Im}\left\{\frac{r_{pp}e^{2ik_z d}}{k_0}\right\}\right], \tag{11}$$

$$M_z(\omega) = (\Theta_{T_p} - \Theta_{T_e})\frac{k_0}{c}\text{Im}\{\alpha_0(\omega)\}\int_0^{\infty}dk_\parallel\int_0^{2\pi}d\phi\frac{k_\parallel}{8\pi^2 k_0}\text{Im}[(r_{sp} + r_{ps})e^{2ik_z d}], \tag{12}$$

$$F_y(\omega) = F_x(\omega, \cos\phi \rightarrow \sin\phi), \qquad M_y(\omega) = M_x(\omega, \cos\phi \rightarrow \sin\phi, \sin\phi \rightarrow -\cos\phi). \tag{13}$$

Total power, force, and torque are obtained by integrating corresponding spectral density over all frequencies as $Q^t = \int_{-\infty}^{\infty}Q(\omega)d\omega/2\pi$ where $Q = \{P, F_j, M_j\}$. The term outside the wave-vector integration in Eq. (8) comes from the heat transfer between the particle and the vacuum half space. Such transfer does not lead to any force or torque for an isotropic particle. The terms inside the wave-vector integration indicate the interaction between the particle and the substrate via quantum- and thermal-fluctuations-generated photons characterized by their frequency ω and in-plane wave-vector components $(k_x = k_\parallel\cos\phi, k_y = k_\parallel\sin\phi)$. Electromagnetic response of the substrate enters through the Fresnel reflection coefficients r_{jk} for $j, k \in [s, p]$ defined above. Here we assume that there are no relative translational or rotational motions between the particle and the substrate. In the presence of such relative motions, Eqs. (8)–(13) will need to be modified to take into account resulting Doppler shift in the frequency of photons being exchanged. The extension of Eqs. (8)–(13) taking into account the rotation of the particle, is provided in Appendix D where we show that the corrections due to such relative motions are in general quite small since these motions are usually in the nonrelativistic regime. Therefore, in practice, Eqs. (8)–(13) are sufficient for achievable exper-

imental situations. We note that the phenomenon of quantum friction or lateral force for moving slabs in relative motion has been previously investigated in Refs. [29,40–42]. While a moving medium can be described by a stationary nonreciprocal magnetoelectric medium for analyzing electromagnetic waves inside it [43], such a description is not applicable for the calculation of fluctuations-induced interactions between moving objects because it does not capture the Doppler frequency shift of the exchanged photons. When all bodies are at the same temperature (thermal equilibrium), a moving slab can cause a lateral Casimir force on a dielectric particle in its vicinity while a stationary nonreciprocal magnetoelectric medium does not lead to such equilibrium lateral force on the particle.

We note that all components of force and torque can be separately derived by dividing the integrand in the power spectral density [Eq. (8)] by the photon energy $\hbar\omega$, multiplying by linear momentum vector $\hbar(k_\parallel\cos\phi, k_\parallel\sin\phi, k z)$ and spin angular momentum vector $\hbar(\sin\phi, -\cos\phi, 0)$ of polaritons, and accounting for whether the photon is emitted or absorbed by the particle. This physically meaningful alternative derivation is exact for force calculation but approximate for torque calculation because the spin angular momentum

$\hbar(\sin\phi, -\cos\phi, 0)$ is exact only for large wave vector polaritons ($k_{\parallel} \gg k_0$) (also proved separately in the Appendix C). The alternative derivation reveals the intimate connection between energy, linear and angular momentum transfer in our system.

Equations (9)–(13) are consistent with some of the general physics constraints. At thermal equilibrium ($\Theta_{T_p} = \Theta_{T_e}$), all force and torque components as predicted by Eqs. (9)–(13) are zero except the perpendicular force F_z. This follows from the observation that the Casimir free energy of the system depends on the vertical displacement d between the particle and the substrate but not the lateral displacement. For a substrate made of reciprocal media, the Fresnel coefficients satisfy the reciprocity constraints $r_{ss,pp}(k_{\parallel}, \phi) = r_{ss,pp}(k_{\parallel}, \phi + \pi)$ and $r_{sp}(k_{\parallel}, \phi) = -r_{ps}(k_{\parallel}, \phi + \pi)$ [24,44]. By integrating Eqs. (9) to (13), it follows that there is no lateral force and no lateral torque on the particle in the near field of a reciprocal medium, for both equilibrium and nonequilibrium scenarios. For a nonreciprocal medium, the reciprocity constraints no longer hold and therefore, one can expect to see nontrivial effects for the nonequilibrium scenarios. Therefore, we consider a substrate made of doped InSb with external magnetic field, which results in a strong nonreciprocity in its electromagnetic response. The reflection coefficients in equations 8 to 13 are obtained by solving the boundary conditions at the interface [16].

III. RESULTS

We consider both a local model and a nonlocal model [16] for the permittivity of InSb to highlight some of the consequences of the nonlocal dielectric response. Figure 2(a) shows the frequency-dependent local permittivity ($\epsilon_{jk}(\omega)$ for $j, k = [x, y, z]$) of InSb slab in presence of magnetic field $B = 1T$ applied along **x** axis. The variation of diagonal components reveals the approximate locations of the surface phonon (higher branch) and plasmon (lower branch) polaritons, henceforth denoted by the acronym SPhP and SPP, respectively. Figure 2(b) shows the polaritonic dispersion ($\omega(k_{\parallel})$) of nonreciprocal SPPs propagating in different directions. Since the behavior is the same for nonreciprocal SPhPs, we focus on SPPs in this figure. As shown in the inset, because of the Zeeman interaction between the spin magnetic moment of nonreciprocal surface polaritons and the magnetic field [19], the polaritons making an angle $\phi \in [0, \pi)$ with B-field and carrying positive momentum $k_y > 0$ experience a redshift whereas the polaritons characterized by $\phi \in [\pi, 2\pi)$ or $k_y < 0$ experience a blueshift compared to the dispersion in the absence of the magnetic field ($B = 0$). Based on the momentum k_y, the red-shifted polaritons can be collectively interpreted as forward waves and blue-shifted polaritons as backward waves. Due to these opposite frequency shifts, the forward and backward momentum waves of equal frequency carry very different momentum and experience unequal near-field coupling with the particle [proportional to $e^{-2|k_z|d}$ in Eqs. (8)–(13)], leading to a lateral force and torque.

Figure. 2(b) shows the SPP dispersion using both a nonlocal model (solid lines) and a local model (dashed lines). At large wave vectors, $\omega(k_{\parallel})$ increases based on a nonlocal model while it reaches a constant value based on a local model.
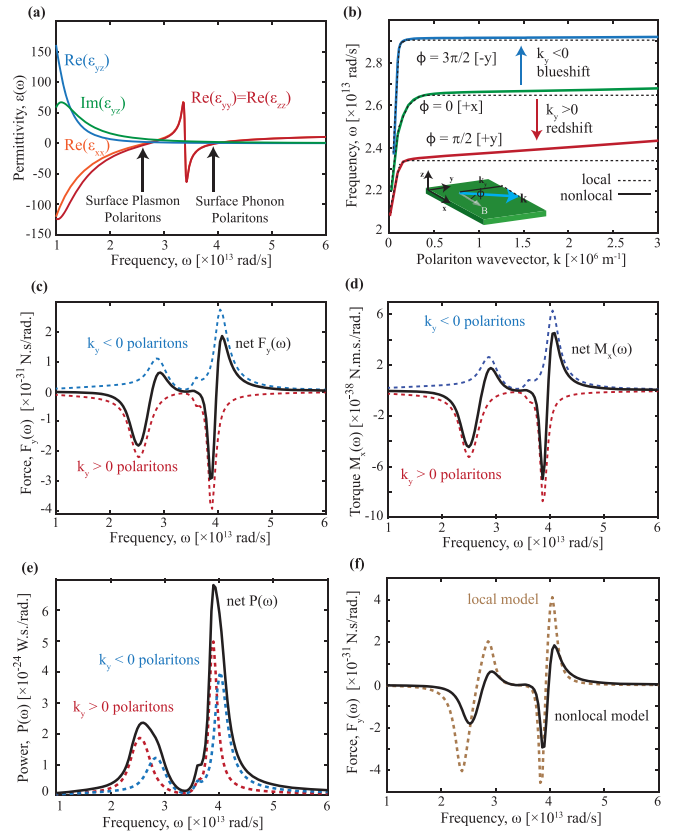

FIG. 2. (a) The frequency-dependent local permittivity of InSb slab in magnetic field $B = 1$ T reveals the approximate locations of surface polaritons. (b) Dispersion $\omega(k_{\parallel})$ for SPPs propagating at an in-plane angle ϕ with B field shows redshift for $\phi \in [0, \pi)$ ($k_y > 0$) and blueshift for $\phi \in [\pi, 2\pi)$ ($k_y < 0$). Dispersion is plotted using both a nonlocal model (solid lines) and a local model (dashed lines). (c) The force spectral density calculated using a nonlocal model for a particle at a distance $d = 0.3\,\mu$m from the slab and under operating temperatures $T_p = 305$ K, $T_e = 300$ K is shown by black line. Its characteristic shape follows from the collective contributions of red-shifted ($k_y > 0$) forward polaritons and blue-shifted ($k_y < 0$) backward polaritons, which are plotted separately as dashed lines. (d) and (e) respectively demonstrate the power and torque spectral densities (black lines). The separately plotted collective contributions of red-shifted and blue-shifted polaritons (dashed lines) clarify the asymmetric flow of energy and angular momenta respectively. (f) shows the force spectral density obtained using local and nonlocal models.

While this reveals a stark contrast between the two models pertaining to presence or absence of strictly unidirectional SPPs [16], we note that the lateral force and torque arise due to opposite frequency shifts of forward and backward waves noted above, which occurs for both local and nonlocal models and does not require strict unidirectionality. Nonetheless, the magnitudes of force and torque are slightly different as we show further below. Unless noted otherwise, all results below are generated using a nonlocal model.

To highlight the effects of the nonreciprocal surface waves, we first calculate the spectral densities in Eqs. (9)–(13) assuming a frequency-independent polarizability, $\text{Im}\{\alpha_0(\omega)\} = 10^{-19}$ m^{-3} for the particle. We use the temperatures

$T_p = 305$ K and $T_e = 300$ K. We find that $F_x(\omega)$, $M_y(\omega)$, and $M_z(\omega)$ are identically zero for this configuration. We do not discuss the perpendicular Casimir force $F_z(\omega)$ here since its behavior is well known, and focus instead on the lateral effects. Figure 2(c) demonstrates the force spectral density (black line) when the center of the particle is at a distance $d = 0.3\,\mu$m from the surface along with the separate collective contributions of red-shifted polaritons (red dashed line) and blue-shifted polaritons (blue dashed line). In the case of $T_p > T_e$, there is a net emission from the particle to the substrate. The emission to red-shifted and blue-shifted polaritons provides a negative ($F_y < 0$) and positive ($F_y > 0$) contribution to the force, from linear momentum conservation, as they carry positive ($k_y > 0$) and negative ($k_y < 0$) momentum, respectively. The difference in these two contributions arising from the nonreciprocity in the dispersion of surface waves, results in the lateral nonequilibrium Casimir force. Figure 2(d) demonstrates the torque spectral density (black line) where the sign of the torque follows from the separate contributions of red-shifted and blue-shifted polaritons carrying positive and negative transverse spin (along **x** axis) respectively, and based on angular momentum conservation. And again, the difference in these two collective contributions causes the lateral nonequilibrium Casimir torque.

Figure 2(e) also highlights the asymmetry in the net power transfer from the particle to forward and backward nonreciprocal surface waves and the resulting spectrally broadened total contribution (black line). Figure 2(f) plots the force spectral density based on local and nonlocal models. The local model overestimates the magnitude of the force and its spectrum is red-shifted compared to that obtained using the nonlocal model. We also note that the strength of nonreciprocity as characterized by the magnitude of ϵ_{yz} shown by blue, green curves in Fig. 2(a) is smaller for SPhP frequencies than for SPP frequencies. Since SPhPs experience low loss than SPPs, the resonant enhancement of nonreciprocity is higher for SPhPs due to higher quality factor than for SPPs, eventually leading to comparable contributions to the spectral densities of power, force, and torque.

To estimate the magnitude of the total lateral force and torque in potential experiments, we consider various nanoparticles (PbTe, AgBr, CdTe, AgCl, NaCl, ZnSe, undoped InAs) of radius $R = 200$ nm whose polarizability response functions are shown in Fig. 3(a). The material permittivity $\epsilon(\omega)$ is obtained from various references [45–47] and the polarizability is calculated as $\alpha(\omega) = 4\pi R^3[\epsilon(\omega) - 1]/[\epsilon(\omega) + 2]$ using a dipolar approximation, which is fairly accurate since the particle radius is much smaller than the relevant wavelengths of 45–90 μm (deep subwavelength regime). The stated materials were chosen because they exhibit a strong resonant response in the aforementioned frequency range. By comparing the resonant frequency of the particle with the frequencies of red-shifted and blue-shifted nonreciprocal SPPs and SPhPs of InSb, we can deduce the directionalities of the lateral force and torque. Assuming warm particles ($T_p > T_e$), it follows that AgBr, PbTe particles experience $F_y^t < 0$ and $M_x^t < 0$ since they emit photons dominantly to red-shifted SPPs while all other particles experience $F_y^t > 0$ and $M_x^t > 0$ since they emit photons dominantly to blue-shifted SPPs or SPhPs. The opposite force behavior for different materials suggests that it
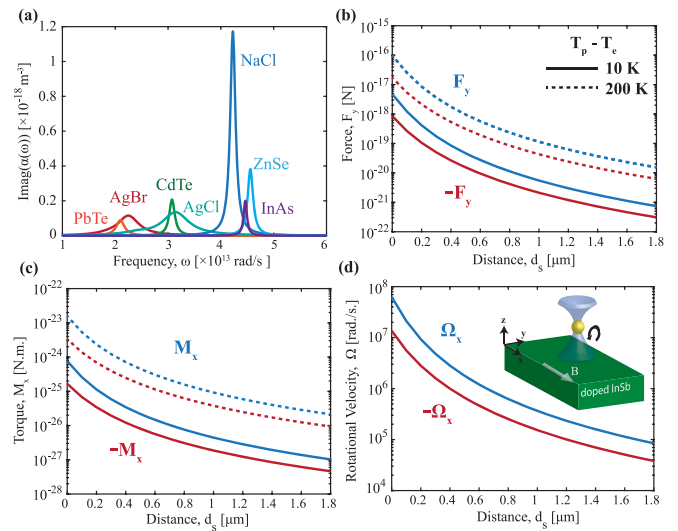

FIG. 3. (a) We consider nanoparticles of radius $R = 200$ nm and made of different materials such that they exhibit dipolar resonances over the frequency range of interest. [(b),(c)] demonstrate the dependence of force and torque on surface-to-surface distance $d_s = d - R$ for AgBr (red) and NaCl (blue) nanoparticles for two different operating temperatures $T_p = 310$ K (solid lines) and $T_p = 500$ K (dashed lines) assuming $T_e = 300$ K. (d) We consider a potential experiment where the same AgBr and NaCl particles are trapped near InSb slab in $B = 1T$ **x** inside a vacuum chamber of pressure 10^{-5} torr. The particles reach a steady state angular velocity at which the lateral torque is balanced by the rotational drag of imperfect vacuum. The figure plots the distance dependence of steady-state rotational velocities for operating temperatures $T_p = 310$ K and $T_e = 300$ K.

might be possible to use such lateral force to sort particles based on the material composition.

Figures 3(b) and 3(c) demonstrate the distance dependence of lateral force and torque on AgBr (red lines) and NaCl (blue lines) particles of radius $R = 200$ nm for temperatures $T_p = 310$ K (solid lines) and $T_p = 500$ K (dashed lines) assuming $T_e = 300$ K. The magnitudes of force and torque increase as the particle's temperature increases. For both choices of T_p, their magnitudes increase as the particle-surface separation decreases. For NaCl particle at $T_p = 500$ K, lateral force $F_y^t \sim 10^{-16}$ N and lateral torque $M_x^t \sim 10^{-23}$ Nm are observed when the vacuum gap spacing between the particle and the substrate is reduced to few nanometers. Such a force is in fact comparable to the force of gravity on the particle. For NaCl particle of mass density $\rho = 2.165$ g/cm^3, gravity force is $W = 7.3 \times 10^{-17}$ N. For AgBr particle of mass density $\rho = 6.47$ g/cm^3, gravity force is $W = 2.17 \times 10^{-16}$ N. Ultrasensitive detection of force of magnitude 10^{-20} N and torque of magnitude 10^{-27} Nm have been realized in experiments [12,13,48,49]. Other recent experiments have measured near-field heat transfer at nanoscale under large temperature differentials [31,32,50–52]. In Ref. [32], temperature differences larger than 100 K were maintained between a tip and a plate separated by 2 nm. Therefore, we are optimistic that the experimental demonstration of our predictions should be feasible.

We also consider an alternative experiment where the particle is optically levitated in the near field of InSb slab inside a vacuum chamber. The particle at temperature $T_p \neq T_e$ experiences a lateral thermal-fluctuations-induced torque M_x, which causes an angular acceleration about **x** axis. As the particle's angular velocity (Ω) increases, there is also an additional damping torque from the residual air molecules inside the vacuum chamber. The damping torque opposes the angular velocity and it can be described as [53,54]

$$M_{\text{damp}} = -\frac{\Omega p_{\text{gas}} \pi (2R)^4}{11.976} \sqrt{\frac{2m_{\text{gas}}}{k_B T_e}} = -\gamma_{\text{damp}} \Omega \qquad (14)$$

where R is the radius of the nanoparticle, $m_{\text{gas}} = 4.8 \times 10^{-26}$ kg is the average mass of air molecule, and p_{gas} is the air pressure. Using the particle's moment of inertia $I_x = \frac{2}{5} m_p R^2$, the evolution of its angular velocity follows the following stochastic equation derived using Brownian theory [55]:

$$d\Omega = \frac{M_x}{I_x} dt - \frac{\gamma_{\text{damp}}}{I_x} \Omega dt + \sqrt{\frac{2\gamma_{\text{damp}} k_B T_e}{I_x^2}} dW \qquad (15)$$

where dW is a normally distributed random number of mean $\langle dW \rangle = 0$ and standard deviation $\langle dW^2 \rangle = dt$ and dt is the time step much smaller than the relaxation timescale $\mathcal{O}(I_x/\gamma_{\text{damp}})$. The term multiplying dW, also known as fluctuation–dissipation theorem (FDT), indicates that the strength of the fluctuations is related to the dissipation or damping rate. This FDT characterizes the mechanical thermal noise, which approximates the stochastic force arising from the interaction of the particle with a large number of the residual air molecules of the chamber. The above equation is simulated using Euler Maruyama method over a large number of trajectories [55]. In the absence of gyrotropy-induced lateral torque ($M_x = 0$), the specific form of FDT ensures that the average rotational energy of the particle given by $\frac{1}{2} I_x \Omega^2$ is equal to $k_B T_e/2$ at equilibrium with the environment at temperature T_e (equipartition law). At equilibrium, the average angular velocity $\langle \Omega \rangle = 0$ and the standard deviation $\sqrt{\langle \Omega^2 \rangle} = k_B T_e/I_x$. For AgBr and NaCl nanoparticles in an environment at $T_e = 300$ K (considered in the main text), the typical standard deviation is $\sqrt{\langle \Omega^2 \rangle} \approx 10^4$ rad/s.

In presence of nonequilibrium lateral torque ($M_x \neq 0$), the steady-state angular velocity is $\Omega_{\text{ss}} = M_x/\gamma_{\text{damp}}$ ignoring the mechanical thermal noise. It is straightforward to numerically verify the intuition that this additional noise in the dynamics can be ignored if $\Omega_{\text{ss}} \gg 10^4$ rad/s (mean standard deviation due to mechanical thermal noise). For realistic vacuum chambers of gas pressure 10^{-5} torr and lateral nonequilibrium

torque $M_x \gtrsim 10^{-27}$ Nm attained in the near-field of InSb slab, we find $\Omega_{\text{ss}} \gg 10^4$ rad/s. For smaller values of torque away from the slab ($M_x < 10^{-27}$ Nm), in general, full numerical simulations including the mechanical thermal noise ($\sim dW$) can be performed for calculating the steady-state mean angular velocity.

Figure 3(d) shows the steady-state rotational velocities $\Omega_{\text{ss}} \gtrsim 10^6$ rad/s for AgBr (red) and NaCl (blue) particles of radius $R = 200$ nm in a vacuum chamber of $p_{\text{gas}} = 10^{-5}$ torr under temperature difference of $T_p - T_e = 10$ K. For the above parameters, the time constant I_x/γ_{damp} is of the order of minutes for AgBr (~ 140 s) and NaCl (~ 48 s) particles. As the magnetic field of $1T$ is turned on at $t = 0$, the particles will reach these steady-state rotational velocities in few minutes. As displayed, the particles rotate with opposite angular velocities and they reach rotational velocities in the MHz-GHz range depending on their distance from the surface. Such rotations could be detected in experiments. We note that the nonreciprocity-induced nonequilibrium torque was recently analyzed for a single gyrotropic particle [29] and for two finite-size gyrotropic particles separated by small distance [30]. The magnitude of the torque in our work is few orders of magnitude larger than the values reported in the previous studies due to the large density of surface polariton states in the near field of a gyrotropic substrate [53]. We also note that the magnitudes of the lateral nonequilibrium fluctuational force and torque can be further enhanced using Weyl semimetals [56], which provide much stronger gyrotropy compared to InSb considered here.

IV. CONCLUSION

We demonstrated that the thermal fluctuations of nonreciprocal surface waves can lead to a lateral force and torque on an isotropic nanoparticle under nonequilibrium conditions. We clarified the origin of these effects by transparently accounting for the underlying asymmetric flow of energy and momenta. We connected the lateral force to the dispersion of nonreciprocal surface polaritons and the lateral torque to the spin-momentum locking. We also made predictions for potential experiments to detect these nonreciprocal fluctuational electrodynamic effects soon. Our paper indicates intriguing opportunities at the intersection of nonreciprocity, photon spin, nonequilibrium statistical physics, and topological materials.

ACKNOWLEDGMENT

APPENDIX A: DERIVATION OF RADIATED POWER

The power exchanged with the vacuum part of the geometry corresponding to the vacuum part of the Green's function [Eq. (4)] is given below:

$$P_{\text{vac}}(\omega) = \frac{\omega^3}{\pi c^3} \text{Im}\{\alpha_0(\omega)\}[\Theta_{T_p} - \Theta_{T_e}]. \qquad (A1)$$

The radiated power corresponding to the reflected part of the Green's function in Eq. (4), henceforth abbreviated as $G_{jk}^{\mathrm{ref}}(\mathbf{r}_1, \mathbf{r}_2, \omega)$, and originating from the particle dipole moment fluctuations [Eq. (6)] is

$$
\begin{aligned}
P_{\mathrm{ref}}^{p}(\omega) &= \omega^3 \mu_0 \mathrm{Im}\big[p_j^{\mathrm{fl}*}(\mathbf{r}_1, \omega)\big(G_{jk}^{\mathrm{ref}}(\mathbf{r}_1, \mathbf{r}_2, \omega)p_k(\mathbf{r}_2, \omega)\big)_{\mathbf{r}_2 \to \mathbf{r}_1}\big] \\
&= \omega^3 \mu_0 \frac{\epsilon_0}{\omega} \Theta_{T_p} \mathrm{Im}\{\alpha_0(\omega)\} \mathrm{Im}\big[\mathrm{Tr}\big(G_{jk}^{\mathrm{ref}}\big)\big] \\
&= \frac{\omega^2}{c^2} \Theta_{T_p} \mathrm{Im}\{\alpha_0\} \mathrm{Im}\bigg[\int \frac{k_\parallel dk_\parallel d\phi}{(2\pi)^2} \frac{i e^{2ik_z d}}{2k_z}\bigg[r_{ss} + r_{pp}\bigg(\frac{2k_\parallel^2}{k_0^2} - 1\bigg)\bigg]\bigg].
\end{aligned}
\tag{A2}
$$

The radiated power corresponding to the reflected part of the Green's function, and originating from the environment field fluctuations [Eq. (7)] is:

$$
\begin{aligned}
P_{\mathrm{ref}}^{\mathrm{env}}(\omega) &= \omega \mathrm{Im}\big[\epsilon_0 \alpha^*(\omega)\langle E_j^{\mathrm{fl}*} E_j^{\mathrm{fl}}\rangle\big] \\
&= \omega \epsilon_0 \mu_0 \omega \Theta_{T_e} \mathrm{Im}\big[\alpha^*(\omega)\mathrm{Im}\big[\mathrm{Tr}\big(G_{jk}^{\mathrm{ref}}\big)\big]\big] \\
&= -\frac{\omega^2}{c^2} \Theta_{T_e} \mathrm{Im}\{\alpha_0\} \mathrm{Im}\bigg[\int \frac{k_\parallel dk_\parallel d\phi}{(2\pi)^2} \frac{i e^{2ik_z d}}{2k_z}\bigg[r_{ss} + r_{pp}\bigg(\frac{2k_\parallel^2}{k_0^2} - 1\bigg)\bigg]\bigg].
\end{aligned}
\tag{A3}
$$

The spectrum of the net radiated power from the particle to the environment provided in Eq. (8) is obtained by adding together the above expressions.

APPENDIX B: DERIVATION OF FORCE

Because of the rotational symmetry of the spherical particle described by isotropic polarizability, the direct interaction of the particle with vacuum does not lead to any torque or force on the particle. Therefore, we focus on the force and torque arising from the reflected part of the Green's function. First, we calculate the force spectrum [Eq. (2)] along **x** (parallel to the slab surface) and **z** direction (perpendicular to the slab surface). The force originating from the environment field fluctuations is

$$
\begin{aligned}
F_x^{\mathrm{env}}(\omega) &= \mathrm{Re}\big[\langle \epsilon_0 \alpha_0 E_j^{\mathrm{fl}} \partial_x E_j^{\mathrm{fl}*}\rangle\big] = \int \frac{d\omega}{2\pi} \mathrm{Re}\big[\langle \epsilon_0 \alpha_0 \underbrace{E_j^{\mathrm{fl}}(\mathbf{r}_1)\partial_{x_2}\ E_j^{\mathrm{fl}*}(\mathbf{r}_2)}_{\text{commuting terms}}\rangle\big]_{\mathbf{r}_2 \to \mathbf{r}_1} \\
&= \mathrm{Re}\big[\langle \epsilon_0 \alpha_0 \partial_{x_2} E_j^{\mathrm{fl}}(\mathbf{r}_1) E_j^{\mathrm{fl}*}(\mathbf{r}_2)\rangle\big]_{\mathbf{r}_2 \to \mathbf{r}_1} \\
&= \epsilon_0 \mathrm{Re}\big[\alpha_0 \partial_{x_2}\langle E_j^{\mathrm{fl}}(\mathbf{r}_1) E_j^{\mathrm{fl}*}(\mathbf{r}_2)\rangle\big]_{\mathbf{r}_2 \to \mathbf{r}_1} \\
&= \epsilon_0 \mu_0 \omega \Theta_{T_e} \mathrm{Re}\bigg[\alpha_0 \frac{(-ik_x)G_{jj}(\mathbf{r}_1, \mathbf{r}_2) - (-ik_x)G_{jj}^*(\mathbf{r}_2, \mathbf{r}_1)}{2i}\bigg]_{\mathbf{r}_2 \to \mathbf{r}_1} \\
&= \frac{\omega}{c^2} \Theta_{T_e} \mathrm{Re}\bigg[-i\alpha_0 \mathrm{Im}\bigg[\mathrm{Tr}\bigg[\int \frac{d^2\mathbf{k}_\parallel}{(2\pi)^2} \frac{ik_x}{2k_z} e^{2ik_z d}[(r_{ss}\hat{\mathbf{e}}_{s+} + r_{ps}\hat{\mathbf{e}}_{p+})\hat{\mathbf{e}}_{s-}^T + (r_{sp}\hat{\mathbf{e}}_{s+} + r_{pp}\hat{\mathbf{e}}_{p+})\hat{\mathbf{e}}_{p-}^T]\bigg]\bigg]\bigg] \\
&= \frac{\omega}{c^2} \Theta_{T_e} \mathrm{Im}\{\alpha_0\} \mathrm{Im}\bigg[\int \frac{k_\parallel dk_\parallel d\phi}{(2\pi)^2} \frac{ik_x e^{2ik_z d}}{2k_z} \cos\phi\bigg[r_{ss} + \bigg(\frac{2k_\parallel^2}{k_0^2} - 1\bigg)r_{pp}\bigg]\bigg].
\end{aligned}
\tag{B1}
$$

Note that for reciprocal media, $r_{ss,pp}(\phi) = r_{ss,pp}(\phi + \pi)$ because of the time-reversal symmetry. It then follows that upon integration over the angle ϕ, the integrand at ϕ cancels with the integrand at $\phi + \pi$ because of $\cos\phi$ term, leading to zero parallel force. For nonreciprocal medium, parallel force is not necessarily zero.

Similarly, the $\hat{\mathbf{e}}_z$ component of the force can be calculated. Instead of $(-ik_x)$ terms in the above derivation, we get $(+ik_z)$ from the Green's function, eventually leading to the following expression:

$$
F_z^{\mathrm{env}}(\omega) = \frac{-\omega}{c^2} \Theta_{T_e} \mathrm{Im}\{\alpha_0\} \mathrm{Im}\bigg[\int \frac{k_\parallel dk_\parallel d\phi}{(2\pi)^2} \frac{i e^{2ik_z d}}{2}\bigg[r_{ss} + \bigg(\frac{2k_\parallel^2}{k_0^2} - 1\bigg)r_{pp}\bigg]\bigg].
\tag{B2}
$$

Note that for reciprocal media, no cancellation over angular integration occurs and the above expression leads to a force perpendicular to the surface for both reciprocal and nonreciprocal media.

We will now calculate the force originating from the particle dipole moment fluctuations:

$$
\begin{aligned}
F_x^{p}(\omega) &= \mathrm{Re}\big[\langle p_j^{\mathrm{fl}} \partial_x E_j^{\mathrm{ind}*}\rangle\big] \\
&= \int \frac{d\omega}{2\pi} \mathrm{Re}\bigg[\langle p_j^{\mathrm{fl}}(\mathbf{r}_1)\partial_{x_2}\underbrace{(\omega^2 \mu_0 G_{jk}(\mathbf{r}_2, \mathbf{r}_1)p_k^{\mathrm{fl}}(\mathbf{r}_1))^*}_{E_j^{\mathrm{ind}}(\mathbf{r}_2)}\rangle\bigg]_{\mathbf{r}_2 \to \mathbf{r}_1}
\end{aligned}
$$

$$= \omega^2 \mu_0 \text{Re}\left[\langle p_j^{\text{fl}}(\mathbf{r}_1) p_k^{\text{fl}*}(\mathbf{r}_1) \rangle \left(\partial_{x_2} G_{jk}^*(\mathbf{r}_2, \mathbf{r}_1) \right)_{\mathbf{r}_2 \to \mathbf{r}_1} \right]$$

$$= \omega^2 \mu_0 \text{Re}\left[\frac{\epsilon_0}{\omega} \Theta_{T_p} \text{Im}\{\alpha_0\} \delta_{jk} \left((-ik_x) G_{jk}^*(\mathbf{r}_2, \mathbf{r}_1) \right)_{\mathbf{r}_2 \to \mathbf{r}_1} \right]$$

$$= \frac{\omega}{c^2} \Theta_{T_p} \text{Im}\{\alpha_0\} \text{Im}[k_x G_{jj}^*(\mathbf{r}_1, \mathbf{r}_1)]$$

$$= \frac{-\omega}{c^2} \Theta_{T_p} \text{Im}\{\alpha_0\} \text{Im}\left[\int \frac{k_\parallel dk_\parallel d\phi}{(2\pi)^2} \frac{ik_\parallel e^{2ik_z d}}{2k_z} \cos\phi \left[r_{ss} + \left(\frac{2k_\parallel^2}{k_0^2} - 1 \right) r_{pp} \right] \right]. \tag{B3}$$

For the calculation of force along $\hat{\mathbf{e}}_z$ direction from particle dipole moment fluctuations, the partial derivative ∂_z leads to $(-ik_z)$ instead of $+ik_z$ (for environment contribution) because of the complex conjugation of the Green's function, i.e., $G_{jj}^*(\mathbf{r}_1, \mathbf{r}_1)$. The final expression for the force is

$$F_z^{\text{p}}(\omega) = \frac{-\omega}{c^2} \Theta_{T_p} \text{Im}\{\alpha_0\} \text{Im}\left[\int \frac{k_\parallel dk_\parallel d\phi}{(2\pi)^2} \frac{ie^{2ik_z d}}{2} \left[r_{ss} + \left(\frac{2k_\parallel^2}{k_0^2} - 1 \right) r_{pp} \right] \right]. \tag{B4}$$

The net parallel and perpendicular fluctuations-induced forces acting on the particle are then obtained and provided in Eqs. (9), (10), and (13).

APPENDIX C: DERIVATION OF TORQUE

Similar to the calculation of force, we calculate the torque using the reflected part of Green's function (indicating photons reflected from the surface). The torque M_x^{env} parallel to the surface and originating from the environment field fluctuations is

$$M_x^{\text{env}}(\omega) = \epsilon_0 \text{Re}[\alpha_0 \langle (E_y E_z^* - E_z E_y^*) \rangle]$$

$$= \int \frac{d\omega}{2\pi} \epsilon_0 \text{Re}[\alpha_0 \times 2i \text{Im}\{E_y E_z^*\}]$$

$$= -2\epsilon_0 \mu_0 \omega \Theta_{T_e} \text{Im}\{\alpha_0\} \text{Im}\left[\frac{G_{yz} - G_{zy}^*}{2i} \right]$$

$$= -\frac{\omega}{c^2} \Theta_{T_e} \text{Im}\{\alpha_0\} \int \frac{d^2\mathbf{k}_\parallel}{(2\pi)^2} \text{Im}\left[\frac{-k_\parallel}{2k_0} \cos\phi \left(r_{sp} \frac{e^{2ik_z d}}{k_z} + r_{ps}^* \frac{e^{-2ik_z^* d}}{k_z^*} \right) - \frac{ik_\parallel}{k_0} \sin\phi \text{Im}\left(r_{pp} \frac{e^{2ik_z d}}{k_0} \right) \right]$$

$$= -\frac{\omega}{c^2} \Theta_{T_e} \text{Im}\{\alpha_0\} \int \frac{k_\parallel dk_\parallel d\phi}{(2\pi)^2} \left[-\frac{k_\parallel}{2k_0} \cos\phi \text{Im}\left((r_{sp} - r_{ps}) \frac{e^{2ik_z d}}{k_z} \right) - \frac{k_\parallel}{k_0^2} \sin\phi \text{Im}\{r_{pp} e^{2ik_z d}\} \right]. \tag{C1}$$

The torque in the direction perpendicular to the surface is

$$M_z^{\text{env}}(\omega) = \text{Re}[\alpha_0 \times 2i \text{Im}\{E_x E_y^*\}]$$

$$= -2\epsilon_0 \mu_0 \omega \Theta_{T_e} \text{Im}\left[\frac{G_{xy} - G_{yx}^*}{2i} \right]$$

$$= -\frac{\omega}{c^2} \Theta_{T_e} \text{Im}\{\alpha_0\} \int \frac{k_\parallel dk_\parallel d\phi}{(2\pi)^2} \frac{1}{2k_0} \text{Im}[(r_{sp} + r_{ps}) e^{2ik_z d}]. \tag{C2}$$

The torque components $M_{x,z}^{\text{p}}$ due to photons generated by particle dipole moment fluctuations are

$$M_x^{\text{p}}(\omega) = \omega^2 \mu_0 \text{Re}[\underbrace{\langle p_y^{\text{fl}} (G_{zy} p_y^{\text{fl}})^* - p_z^{\text{fl}} (G_{yz} p_z^{\text{fl}})^* \rangle}_{\text{correlations between dipole moments}}]$$

$$= \omega^2 \mu_0 \frac{\epsilon_0}{\omega} \Theta_{T_p} \text{Im}\{\alpha_0\} \text{Re}[G_{zy}^* - G_{yz}^*]$$

$$= \frac{\omega}{c^2} \Theta_{T_p} \text{Im}\{\alpha_0\} \text{Im}[iG_{zy}^* - iG_{yz}^*]$$

$$= 2\frac{\omega}{c^2} \Theta_{T_p} \text{Im}\{\alpha_0\} \text{Im}\left[\frac{G_{yz} - G_{zy}^*}{2i} \right]$$

$$= \frac{\omega}{c^2} \Theta_{T_p} \text{Im}\{\alpha_0\} \int \frac{k_\parallel dk_\parallel d\phi}{(2\pi)^2} \left[-\frac{k_\parallel}{2k_0} \cos\phi \text{Im}\left((r_{sp} - r_{ps}) \frac{e^{2ik_z d}}{k_z} \right) - \frac{k_\parallel}{k_0^2} \sin\phi \text{Im}\{r_{pp} e^{2ik_z d}\} \right]. \tag{C3}$$

The torque along **z** direction is

$$M_z^{\mathrm{p}}(\omega) = 2\frac{\omega}{c^2}\Theta_{T_p}\mathrm{Im}\{\alpha_0\}\mathrm{Im}\left[\frac{G_{xy}-G_{yx}^*}{2i}\right]$$

$$= \frac{\omega}{c^2}\Theta_{T_p}\mathrm{Im}\{\alpha_0\}\int\frac{k_\parallel dk_\parallel d\phi}{(2\pi)^2}\frac{1}{2k_0}\mathrm{Im}[(r_{sp}+r_{ps})e^{2ik_z d}]. \tag{C4}$$

We then obtain the final expressions for the fluctuations-induced torque spectrum provided in Eqs. (11), (12), and (13).

For reciprocal media, $r_{ss,pp}(\theta,\phi)=r_{ss,pp}(\theta,\phi+\pi)$ and $r_{sp}(\theta,\phi)=-r_{ps}(\theta,\phi)$. By summing the integrands at ϕ and $\phi+\pi$, it follows that particle does not experience any torque. For InSb slab with magnetic field parallel to the surface, this is no longer true and a lateral torque parallel to surface is observed. However, the Fresnel coefficients for this system also satisfy the condition $r_{sp}+r_{ps}=0$ [24] leading to a zero torque along **z** axis.

We note that all components of force and torque can be derived by dividing the integrand in the power spectrum by energy $\hbar\omega$, multiplying by linear momentum vector $\hbar(k_\parallel\cos\phi, k_\parallel\sin\phi, k_z)$ and spin angular momentum vector $\hbar(\sin\phi, -\cos\phi, 0)$ of polaritons, and accounting for whether the photon is emitted or absorbed by the particle. This physically meaningful alternative derivation is exact for force calculation, which is evident from the final expressions of the spectra above. It is approximate for torque because the spin angular momentum $\hbar(\sin\phi, -\cos\phi, 0)$ is exact only for large wave-vector polaritons ($k_\parallel \gg k_0$). This is proved in the following. We can calculate the angular momentum transferred for each photon exchanged, which is characterized by $(\omega, k_\parallel, \phi)$:

$$M_x(\omega, k_\parallel, \phi) = \hbar\frac{\left[\frac{k_\parallel}{2k_0}\cos\phi\,\mathrm{Im}\left((r_{sp}-r_{ps})\frac{e^{2ik_z d}}{k_z}\right) + \frac{k_\parallel}{k_0^2}\sin\phi\,\mathrm{Im}\{r_{pp}e^{2ik_z d}\}\right]}{\mathrm{Im}\left[\frac{ie^{2ik_z d}}{2k_z}[r_{ss}+r_{pp}\left(\frac{2k_\parallel^2}{k_0^2}-1\right)]\right]} \tag{C5}$$

$$M_y(\omega, k_\parallel, \phi) = \hbar\frac{\left[\frac{k_\parallel}{2k_0}\sin\phi\,\mathrm{Im}\left((r_{sp}-r_{ps})\frac{e^{2ik_z d}}{k_z}\right) - \frac{k_\parallel}{k_0^2}\cos\phi\,\mathrm{Im}\{r_{pp}e^{2ik_z d}\}\right]}{\mathrm{Im}\left[\frac{ie^{2ik_z d}}{2k_z}[r_{ss}+r_{pp}\left(\frac{2k_\parallel^2}{k_0^2}-1\right)]\right]}. \tag{C6}$$

For evanescent waves ($k_\parallel > k_0$), $k_z = i|k_z|$ is purely imaginary, which simplifies the above expressions:

$$M_x(\omega, k_\parallel, \phi) = \hbar\frac{\left[\frac{k_\parallel}{2k_0|k_z|}\cos\phi\,\mathrm{Re}\left(-(r_{sp}-r_{ps})\right) + \frac{k_\parallel}{k_0^2}\sin\phi\,\mathrm{Im}\{r_{pp}\}\right]}{\left[\frac{\mathrm{Im}(r_{ss})}{2|k_z|} + \frac{\mathrm{Im}(r_{pp})}{2|k_z|}\left(\frac{2k_\parallel^2}{k_0^2}-1\right)\right]} \tag{C7}$$

$$M_y(\omega, k_\parallel, \phi) = \hbar\frac{\left[\frac{k_\parallel}{2k_0|k_z|}\sin\phi\,\mathrm{Re}\left(-(r_{sp}-r_{ps})\right) - \frac{k_\parallel}{k_0^2}\cos\phi\,\mathrm{Im}\{r_{pp}\}\right]}{\left[\frac{\mathrm{Im}(r_{ss})}{2|k_z|} + \frac{\mathrm{Im}(r_{pp})}{2|k_z|}\left(\frac{2k_\parallel^2}{k_0^2}-1\right)\right]}. \tag{C8}$$

For evanescent waves carrying large momentum $k_\parallel \gg k_0$, which leads to $|k_z| \approx k_\parallel$, the above expressions further simplify to:

$$M_x(\omega, k_\parallel \gg k_0, \phi) = (\sin\phi)\hbar,$$
$$M_y(\omega, k_\parallel \gg k_0, \phi) = (-\cos\phi)\hbar. \tag{C9}$$

APPENDIX D: ANGULAR VELOCITY DEPENDENCE OF THE TORQUE

We note that, in the derivation provided above, the lateral torque M_x is derived for a non-rotating particle. The effect of the particle's rotational velocity Ω on the magnitude of this torque is negligible as long as its rotational velocity is much smaller than the emission frequencies ($\Omega \ll \omega$). For our situation, $\omega \sim 10^{13}$ rad/s while $\Omega_{ss} \sim 10^7$ rad/s and hence ignoring the dependence of M_x on Ω is justified. Nonetheless, we derive $M_x(\Omega)$ below and prove this point. We follow the derivation similar to that of Ref. [36] for the calculation of torque on rotating particles. The torque originating from the particle's dipole moment fluctuations is calculated in the laboratory frame. For a particle rotating at angular velocity Ω

about **x** axis, the fluctuating dipole moments in the laboratory frame p_j^l are related to the fluctuating dipole moments in the rotating frame p_j^{fl} (FDT is well defined in the rotating frame [36]) as:

$$p_y^l = \tfrac{1}{2}\left[p_{y,\omega}^{\mathrm{fl}}e^{-i\omega_- t} + p_{y,\omega}^{\mathrm{fl}}e^{-i\omega_+ t} + p_{y,\omega}^{\mathrm{fl*}}e^{i\omega_+ t} + p_{y,\omega}^{\mathrm{fl*}}e^{i\omega_- t}\right.$$
$$\left. + ip_{z,\omega}^{\mathrm{fl}}e^{-i\omega_- t} - ip_{z,\omega}^{\mathrm{fl}}e^{-i\omega_+ t} + ip_{z,\omega}^{\mathrm{fl*}}e^{i\omega_+ t} - ip_{z,\omega}^{\mathrm{fl*}}e^{i\omega_- t}\right],$$

$$p_z^l = \tfrac{1}{2}\left[-ip_{y,\omega}^{\mathrm{fl}}e^{-i\omega_- t} + ip_{y,\omega}^{\mathrm{fl}}e^{-i\omega_+ t} - ip_{y,\omega}^{\mathrm{fl*}}e^{i\omega_+ t}\right.$$
$$\left. + ip_{y,\omega}^{\mathrm{fl*}}e^{i\omega_- t} + p_{z,\omega}^{\mathrm{fl}}e^{-i\omega_- t} + p_{z,\omega}^{\mathrm{fl}}e^{-i\omega_+ t} + p_{z,\omega}^{\mathrm{fl*}}e^{i\omega_+ t}\right.$$
$$\left. + p_{z,\omega}^{\mathrm{fl*}}e^{i\omega_- t}\right],$$

$$p_x^l = p_{x,\omega}^{\mathrm{fl}}e^{-i\omega t} + p_{x,\omega}^{\mathrm{fl*}}e^{i\omega t},$$

where $\omega_\pm = \omega \pm \Omega$ and both positive and negative frequencies are considered together such that the final integration is performed only over positive frequencies ($\int_0^\infty d\omega/2\pi$). The fluctuating dipole moments $p_{j,\omega}^{\text{fl}}$ satisfy the FDTs above and are used to calculate the resulting torque. This calculation also requires induced electric fields, which are obtained using the Green's function [$E_j^{\text{ind}} = G_{jk,\omega} p_{k,\omega_m}^{\text{fl}} e^{-i\omega_m t}$ for $\omega_m \in [\omega, \omega_+, \omega_-]$ and its complex conjugate].

The calculation of torque originating from the electric field fluctuations requires the electric fields in the rotating frame of the particle. For the particle rotating at angular velocity Ω, the field fluctuations E_j^r in the rotating frame are

$$E_y^r = \frac{1}{2}\big[E_{y,\omega}^{\text{fl}} e^{-i\omega_- t} + E_{y,\omega}^{\text{fl}} e^{-i\omega_+ t} + E_{y,\omega}^{\text{fl}*} e^{i\omega_+ t} + E_{y,\omega}^{\text{fl}*} e^{i\omega_- t}$$
$$- iE_{z,\omega} e^{-i\omega_- t} + iE_{z,\omega} e^{-i\omega_+ t} - iE_{z,\omega}^{\text{fl}*} e^{i\omega_+ t} + iE_{z,\omega}^{\text{fl}*} e^{i\omega_- t}\big],$$

$$E_z^r = \frac{1}{2}\big[iE_{y,\omega}^{\text{fl}} e^{-i\omega_- t} - iE_{y,\omega}^{\text{fl}} e^{-i\omega_+ t} + iE_{y,\omega}^{\text{fl}*} e^{i\omega_+ t} - iE_{y,\omega}^{\text{fl}*} e^{i\omega_- t}$$
$$+ E_{z,\omega}^{\text{fl}} e^{-i\omega_- t} + E_{z,\omega}^{\text{fl}} e^{-i\omega_+ t} + E_{z,\omega}^{\text{fl}*} e^{i\omega_+ t} + E_{z,\omega}^{\text{fl}*} e^{i\omega_- t}\big],$$

$$E_x^r = E_{x,\omega}^{\text{fl}} e^{-i\omega t} + E_{x,\omega}^{\text{fl}*} e^{i\omega t}.$$

Using the induced dipole moments in the rotating frame, $p_j^{r,\text{ind}} = \epsilon_0 \alpha_0 E_j^r$, the torque due to electric field fluctuations can be obtained. After some straightforward algebra, we get the following torque due to the reflected part of the Green's function:

$$M_x^e = \frac{\epsilon_0 \Theta_{T_e}}{\omega}\big[\text{Im}(\alpha_{\omega_-} + \alpha_{\omega_+})\text{Re}\big(G_{yz,\omega}^t - G_{zy,\omega}^t\big)$$
$$+ \text{Im}\big(G_{yy}^t + G_{zz}^t\big)\text{Im}(\alpha_{\omega_-} - \alpha_{\omega_+})\big], \quad \text{(D1)}$$

$$M_x^p = \frac{\epsilon_0 \Theta_{T_p}}{\omega}\text{Im}(\alpha_\omega)\big[\text{Im}\big(G_{zz,\omega_-}^t - G_{zz,\omega_+}^t\big)$$
$$+ \text{Im}\big(G_{yy,\omega_-}^t - G_{yy,\omega_+}^t\big) - \text{Re}\big(G_{yz,\omega_+}^t - G_{zy,\omega_+}^t\big)$$
$$- \text{Re}\big(G_{yz,\omega_-}^t - G_{zy,\omega_-}^t\big)\big], \quad \text{(D2)}$$

where $G^t = \omega^2 \mu_0 G$ is used for simplifying the expressions. The subscripts indicate the frequencies at which the related terms are to be evaluated. The required expressions for G^t are

$$G_{yz,\omega}^t - G_{zy,\omega}^t = \omega^2 \mu_0 \int \frac{k_\parallel dk_\parallel d\phi}{(2\pi)^2} \frac{ie^{2ik_z d}}{2k_z}$$
$$\times \left[-(r_{sp} - r_{ps})\frac{k_\parallel}{k_0}\cos\phi - 2r_{pp}\frac{k_\parallel k_z}{k_0^2}\right],$$

$$G_{yy,\omega}^t = \omega^2 \mu_0 \int \frac{k_\parallel dk_\parallel d\phi}{(2\pi)^2} \frac{ie^{2ik_z d}}{2k_z}$$
$$\times \left[r_{ss}\cos^2\phi + (r_{ps} - r_{sp})\frac{k_z}{k_0}\sin\phi\cos\phi\right.$$
$$\left. - r_{pp}\frac{k_z^2}{k_0^2}\sin^2\phi\right],$$

$$G_{zz,\omega}^t = \omega^2 \mu_0 \int \frac{k_\parallel dk_\parallel d\phi}{(2\pi)^2} \frac{ie^{2ik_z d}}{2k_z} r_{pp}\frac{k_\parallel^2}{k_0^2}.$$

The torque because of the vacuum part of the Green's function [Eq. (4)] (indicating direct interaction with vacuum half-
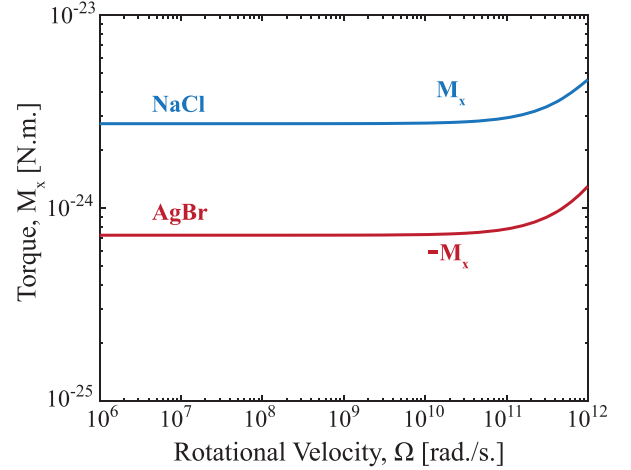

FIG. 4. Figure shows the angular velocity dependence of the lateral nonequilibrium torque on AgBr (red) and NaCl (blue) nanoparticle of $R = 200$ nm at a distance $d_s = 100$ nm from the surface of InSb half-space in $B = 1T$ magnetic field along **x**. The operating temperatures are $T_p = 400$ K and $T_e = 300$ K. The magnitude of the torque is affected appreciably at large angular velocities of $\Omega \sim \mathcal{O}(10^{11})$rad/s because the rotational Doppler effect on thermal emission dominant at THz frequencies ($\omega \gtrsim 10^{12}$ rad/s) is nonnegligible.

space) is

$$M_x^{e,\text{vac}} = \frac{\epsilon_0 \Theta_{T_e}}{\omega}\text{Im}(\alpha_{\omega_-} - \alpha_{\omega_+})\frac{2\omega^3}{3\pi\epsilon_0 c^3}$$
$$= \frac{2\omega^2}{3\pi c^3}\text{Im}(\alpha_{\omega_-} - \alpha_{\omega_+})\Theta_{T_e}, \quad \text{(D3)}$$

$$M_x^{p,\text{vac}} = \frac{\epsilon_0 \Theta_{T_p}}{\omega}\text{Im}(\alpha_\omega)\frac{2(\omega_-^3 - \omega_+^3)}{3\pi\epsilon_0 c^3}$$
$$= \frac{2(\omega_-^3 - \omega_+^3)}{3\pi\omega c^3}\text{Im}(\alpha_\omega)\Theta_{T_p}. \quad \text{(D4)}$$

In the following, we use the above expressions to compute the lateral torque for the case of AgBr and NaCl particles considered in the main text.

As explained in the main text, we focus on two cases of AgBr and NaCl nanoparticles of radius $R = 200$ nm in the near-field of doped InSb slab in magnetic field $B = 1T$ along **x** axis of the geometry. The particles experience oppositely directed lateral nonequilibrium torque and hence rotate with opposite angular velocities. Figure 4 demonstrates the dependence of the fluctuations-induced torque on the angular velocity of the particle. For this demonstration, we assumed both particles to be at surface-to-surface distance $d_s = 0.1 \, \mu$m. from the slab surface and at temperature $T_p = 400$ K. The temperature of the surrounding environment is $T_e = 300$ K. Intuitively, it follows from the above torque expressions containing terms such as $\omega_\pm = \omega \pm \Omega$ that the angular velocity will alter the magnitude of the torque only when it is comparable to the emission frequencies, which lie in the THz range. This is evident from Fig. 4 where the torque is constant for rotation velocities less than $\Omega = 10^{10}$ rad/s. For particles reaching the rotation speeds beyond these values, the above expressions capturing angular-velocity-dependent

torque must be used. However, since the damping torque of the imperfect vacuum chamber balances the lateral nonequilibrium torque at smaller rotation speeds in the MHz to GHz range, it suffices to use the torque expressions derived for steady particles. We also note that at rotation speeds beyond 10GHz where the effect of the rotation speed on the magnitude of the torque is noticeable, the particle may disintegrate because of the centrifugal stress. These effects depend on the ultimate tensile strength of the material, and must be taken into account at these high rotational velocities [54,57].

[1] R. Camley, Surf. Sci. Rep. **7**, 103 (1987).

[2] Z. Yu, G. Veronis, Z. Wang, and S. Fan, Phys. Rev. Lett. **100**, 023902 (2008).

[3] F. D. M. Haldane and S. Raghu, Phys. Rev. Lett. **100**, 013904 (2008).

[4] Z. Wang, Y. Chong, J. Joannopoulos, and M. Soljačić, Nature (London) **461**, 772 (2009).

[5] Z. Wang, Y. D. Chong, J. D. Joannopoulos, and M. Soljačić, Phys. Rev. Lett. **100**, 013905 (2008).

[6] X. Zhang, A. Galda, X. Han, D. Jin, and V. M. Vinokur, Phys. Rev. Applied **13**, 044039 (2020).

[7] S. A. Hassani Gangaraj, G. W. Hanson, M. G. Silveirinha, K. Shastri, M. Antezza, and F. Monticone, Phys. Rev. B **99**, 245414 (2019).

[8] L. Lu, J. Joannopoulos, and M. Soljačić, Nat. Photonics **8**, 821 (2014).

[9] M. G. Silveirinha, Phys. Rev. B **94**, 205105 (2016).

[10] B. Hu, Y. Zhang, and Q. J. Wang, Nanophotonics **4**, 383 (2015).

[11] B. Bahari, A. Ndao, F. Vallini, A. El Amili, Y. Fainman, and B. Kanté, Science **358**, 636 (2017).

[12] T. Gong, M. Corrado, A. Mahbub, C. Shelden, and J. Munday, Nanophoton. **10**, 523 (2020).

[13] G. Bimonte, T. Emig, M. Kardar, and M. Krüger, Annu. Rev. Condens. Matter Phys. **8**, 119 (2017).

[14] T. Van Mechelen and Z. Jacob, Optica **3**, 118 (2016).

[15] K. Y. Bliokh, D. Smirnova, and F. Nori, Science **348**, 1448 (2015).

[16] S. Buddhiraju, Y. Shi, A. Song, C. Wojcik, M. Minkov, I. Williamson, A. Dutt, and S. Fan, Nat. Commun. **11**, 674 (2020).

[17] L. Zhu and S. Fan, Phys. Rev. Lett. **117**, 134303 (2016).

[18] P. Ben-Abdallah, Phys. Rev. Lett. **116**, 084301 (2016).

[19] C. Khandekar and Z. Jacob, New J. Phys. **21**, 103030 (2019).

[20] C. Guo and S. Fan, Phys. Rev. B **102**, 085401 (2020).

[21] B. Zhao, C. Guo, C. Garcia, P. Narang, and S. Fan, Nano Lett. **20**, 1923 (2020).

[22] A. Ott, R. Messina, P. Ben-Abdallah, and S.-A. Biehs, Appl. Phys. Lett. **114**, 163105 (2019).

[23] E. Moncada-Villa and J. C. Cuevas, Phys. Rev. B **101**, 085411 (2020).

[24] C. Khandekar, F. Khosravi, Z. Li, and Z. Jacob, New J. Phys. **22**, 123005 (2020).

[25] S. A. H. Gangaraj, M. G. Silveirinha, G. W. Hanson, M. Antezza, and F. Monticone, Phys. Rev. B **98**, 125146 (2018).

[26] R. R. Q. P. T. Oude Weernink, P. Barcellona, and S. Buhmann, Phys. Rev. A **97**, 032507 (2018).

[27] F. Lindel, G. W. Hanson, M. Antezza, and S. Y. Buhmann, Phys. Rev. B **98**, 144101 (2018).

[28] D. Gelbwaser-Klimovsky, N. Graham, M. Kardar, and M. Krüger, Phys. Rev. Lett. **126**, 170401 (2021).

[29] Y. Guo and S. Fan, ACS Photonics **8**, 1623 (2021).

[30] X. Gao, C. Khandekar, Z. Jacob, and T. Li, Phys. Rev. B **103**, 125424 (2021).

[31] A. Narayanaswamy, S. Shen, and G. Chen, Phys. Rev. B **78**, 115303 (2008).

[32] K. Kim, B. Song, V. Fernández-Hurtado, W. Lee, W. Jeong, L. Cui, D. Thompson, J. Feist, M. Reid, F. J. García-Vidal, J. C. Cuevas, E. Meyhofer, and P. Reddy, Nature (London) **528**, 387 (2015).

[33] F. Chen, U. Mohideen, G. L. Klimchitskaya, and V. M. Mostepanenko, Phys. Rev. Lett. **88**, 101801 (2002).

[34] T. Emig, A. Hanke, R. Golestanian, and M. Kardar, Phys. Rev. A **67**, 022114 (2003).

[35] F. Bao, K. Shi, G. Cao, J. S. Evans, and S. He, Phys. Rev. Lett. **121**, 130401 (2018).

[36] A. Manjavacas, F. J. Rodríguez-Fortuño, F. J. García de Abajo, and A. V. Zayats, Phys. Rev. Lett. **118**, 133605 (2017).

[37] B. Müller and M. Krüger, Phys. Rev. A **93**, 032511 (2016).

[38] C. Henkel, K. Joulain, J.-P. Mulet, and J.-J. Greffet, J. Opt. A: Pure Appl. Opt. **4**, S109 (2002).

[39] L. D. Landau and E. M. Lifshitz, *Course of Theoretical Physics: Statistical Physics Part 1* (Elsevier, Amsterdam, 2013).

[40] J. B. Pendry, New J. Phys. **12**, 033028 (2010).

[41] U. Leonhardt, New J. Phys. **12**, 068001 (2010).

[42] A. I. Volokitin and B. N. J. Persson, Phys. Rev. Lett. **106**, 094502 (2011).

[43] J. A. Kong, *Theory of Electromangetic Waves* (Wiley Interscience, New York, 1975).

[44] G. Bimonte and E. Santamato, Phys. Rev. A **76**, 013810 (2007).

[45] E. D. Palik, *Handbook of Optical Constants of Solids*, Vol. 3 (Academic Press, New York, 1998).

[46] S. Foteinopoulou, G. C. R. Devarapu, G. S. Subramania, S. Krishna, and D. Wasserman, Nanophotonics **8**, 2129 (2019).

[47] J. D. Caldwell, L. Lindsay, V. Giannini, I. Vurgaftman, T. L. Reinecke, S. A. Maier, and O. J. Glembocki, Nanophotonics **4**, 44 (2015).

[48] M. Antognozzi, C. Bermingham, R. Harniman, S. Simpson, J. Senior, R. Hayward, H. Hoerber, M. Dennis, A. Bekshaev, K. Bliokh, and F. Nori, Nat. Phys. **12**, 731 (2016).

[49] J. Gieseler, L. Novotny, and R. Quidant, Nat. Phys. **9**, 806 (2013).

[50] G. R. Bhatt, B. Zhao, S. Roberts, I. Datta, A. Mohanty, T. Lin, J.-M. Hartmann, R. St-Gelais, S. Fan, and M. Lipson, Nat. Commun. **11**, 2545 (2020).

[51] J. DeSutter, L. Tang, and M. Francoeur, Nat. Nanotechnol. **14**, 751 (2019).

[52] M. Ghashami, H. Geng, T. Kim, N. Iacopino, S. K. Cho, and K. Park, Phys. Rev. Lett. **120**, 175901 (2018).

[53] Z. Xu, Z. Jacob, and T. Li, Nanophoton. **10**, 537 (2020).

[54] J. Ahn, Z. Xu, J. Bang, Y.-H. Deng, T. M. Hoang, Q. Han, R.-M. Ma, and T. Li, Phys. Rev. Lett. **121**, 033603 (2018).

[55] D. J. Higham, SIAM Rev. **43**, 525 (2001).

[56] O. V. Kotov and Y. E. Lozovik, Phys. Rev. B **98**, 195446 (2018).

[57] R. Reimann, M. Doderer, E. Hebestreit, R. Diehl, M. Frimmer, D. Windey, F. Tebbenjohanns, and L. Novotny, Phys. Rev. Lett. **121**, 033602 (2018).